Farnesyl Protein Transferase: Identification of K164α and Y300β as Catalytic Residues by Mutagenesis and Kinetic Studies†

Zhen Wu,*,‡ Mark Demma,‡ Corey L. Strickland,‡ Evette S. Radisky,§ C. Dale Poulter,§ Hung V. Le,‡ and William T. Windsor‡

Schering-Plough Research Institute, 2015 Galloping Hill Road, Kenilworth, New Jersey 07033, and Department of Chemistry, University of Utah, Salt Lake City, Utah 84112

Received March 12, 1999; Revised Manuscript Received June 16, 1999

ABSTRACT: Farnesyl protein transferase (FPT) is an α/β heterodimeric zinc enzyme that catalyzes posttranslational farnesylation of many key cellular regulatory proteins, including oncogenic Ras. On the basis of the recently reported crystal structure of FPT complexed with a CVIM peptide and α-hydroxyfarnesylphosphonic acid, site-directed mutagenesis of the FPT active site was performed so key residues that are responsible for substrate binding and catalysis could be identified. Eight single mutants, including K164Nα, Y166Fα, Y166Aα, Y200Fα, H201Aα, H248Aβ, Y300Fβ, and Y361Fβ, and a double mutant, H248Aβ/Y300Fβ, were prepared. Steady-state kinetic analysis along with structural evidence indicated that residues Y200α, H201α, H248β, and Y361β are mainly involved in substrate binding. In addition, biochemical results confirm structural observations which show that residue Y166α plays a key role in stabilizing the active site conformation of several FPT residues through cation−π interactions. Two mutants, K164Nα and Y300Fβ, have moderately decreased catalytic constants (k_{cat}). Pre-steady-state kinetic analysis of these mutants from rapid quench experiments showed that the chemical step rate constant was reduced by 41- and 30-fold, respectively. The product-releasing rate for each dropped approximately 10-fold. In pH-dependent kinetic studies, Y300Fβ was observed to have both acidic and basic pK_a values shifted 1 log unit from those of the wild-type enzyme, consistent with a possible role for Y300β as an acid−base catalyst. K164Nα had a pK_a shift from 6.0 to 5.3, which suggests it may function as a general acid. On the basis of these results along with structural evidence, a possible FPT reaction mechanism is proposed with both Y300β and K164α playing key catalytic roles in enhancing the reactivity of the farnesyl diphosphate leaving group.

Posttranslational prenylation is an essential process for the functional maturation of many eukaryotic proteins, including Ras and Ras-related proteins (Rap, Rab, Rac, and Ral), the γ-subunit of large G proteins, nuclear lamins, rhodopsin kinase, and the retinal cGMP phosphodiesterases (*1*). Prenylation promotes protein localization to the plasma membrane where specific protein−protein interactions are necessary for advancing signal transduction pathways. Protein prenyltransferases such as farnesyl protein transferase (FPT)[1] or geranylgeranyl protein transferase I (GGPT I) attach a C_{15} farnesyl or C_{20} geranylgeranyl group, respectively, onto the C-terminal motif of proteins containing amino acid sequences of CaaX, where C is cysteine, "a" is an aliphatic amino acid, and X is a residue that determines protein substrate specificity (*1*). FPT has recently become a target for therapeutic intervention because inhibition of the oncogenic p21 Ras farnesylation has been shown to be a potential anticancer therapy (*2*). FPT inhibitors are able to reverse the neoplastic phenotype of human tumor cell lines containing mutated *ras* genes (*3*−*5*) as well as allow complete tumor regression in mice bearing oncogenic *H-ras*-induced tumors (*6*).

FPT catalyzes the transfer of the C_{15} farnesyl group from farnesyl diphosphate (FPP) to proteins where the X residue in the CaaX motif is Ser, Met, Ala, Cys, or Gln (*1*). The genes encoding FPT have been cloned from rat (*7*, *8*), human (*9*), and yeast (*10*). GGPT I utilizes geranylgeranyl diphosphate as a substrate and catalyzes the C_{20} geranylgeranylation of CaaX-containing proteins where the X residue is primarily Leu or Phe (*11*−*14*). FPT and GGPT I are α/β heterodimeric zinc metalloenzymes (*15*) which share an identical α-subunit, but have distinct β-subunits whose sequences are 30% homologous.

Steady-state kinetic analysis and dead-end inhibition studies of human FPT have established that substrate binding

† The research at the University of Utah was supported by NIH Grant GM21328.

* To whom correspondence should be addressed: Schering-Plough Research Institute, K15-2-2945, 2015 Galloping Hill Road, Kenilworth, NJ 07033. Phone: (908) 740-3404. Fax: (908) 740-4844. E-mail: zhen.wu@spcorp.com.

‡ Schering-Plough Research Institute.

§ University of Utah.

[1] Abbreviations: αHFP, α-hydroxyfarnesylphosphonic acid; BME, β-mercaptoethanol; BSA, bovine serum albumin; CaaX, a sequence motif consisting of an invariant cysteine residue fourth from the C-terminus; CD, circular dichroism; DTT, dithiothreitol; EDTA, ethylenediaminetetraacetic acid; FPP, farnesyl diphosphate; FPT, farnesyl protein transferase; GGPT, geranylgeranyl protein transferase; ORF, open reading frame; PAGE, polyacrylamide gel electrophoresis; PCR, polymerase chain reaction; PEP, a CaaX-containing peptide substrate; SDS, sodium dodecyl sulfate; SPA, scintillation proximity assay; Tris, tris(hydroxymethyl)aminomethane.

10.1021/bi990583t CCC: $18.00
Published on Web 08/11/1999

is sequentially ordered with FPP binding first to the enzyme active site, followed by the CaaX-containing protein substrate (*16*, *17*). The resulting ternary complex undergoes a chemical transformation, and reaction products are released from the active site. Pre-steady-state kinetic experiments using rat FPT indicated that FPP binds to the enzyme to form a binary E·FPP complex in a two-step process. In this system, biotinylated GLPCVVM reacted with E·FPP irreversibly at a rate of 2.2×10^5 M^{-1} s^{-1} (*17*). The rate-limiting step in the reaction, reflected by a k_{cat} value of 0.06 s^{-1} at 25 °C, was product release. The slowest step in yeast FPT was also product release; however, the rate constant for the chemical reaction step was only 3-fold faster than that of product release (*18*).

Several studies have been performed in an effort to elucidate the FPT reaction mechanism. On the basis of experiments using a series of fluoro-substituted FPP analogues and transition-state analogues, an electrophilic alkylation mechanism has been proposed for yeast FPT (*19*, *20*). Spectroscopic studies with the Co^{2+}-substituted rat FPT indicated that the nucleophile in the reaction is a Zn^{2+} thiolate of the cysteine residue in the substrate (*21*, *22*). NMR analysis of the stereochemical course in human FPT has established that C1 of FPP undergoes an inversion of configuration during farnesylation (*23*). With these observations and the recently reported three-dimensional crystal structure of rat FPT complexed with a CVIM peptide and an FPP analogue (*24*), additional studies can be performed to elucidate the enzymatic reaction mechanism.

In the reported X-ray structures, either FPP (*25*) or an FPP analogue, α-hydroxyfarnesylphosphonic acid (αHFP) (*24*), binds to FPT in an extended conformation with the isoprenoid chain packing against mainly aromatic residues and the phosphate moieties interacting extensively with positively charged side chains and solvent molecules. The CVIM peptide substrate, acetyl-Cys-Val-Ile-selenoMet-COOH, exhibits an extended conformation and makes interactions with the protein primarily through its side chains. The cysteine thiol, which reacts with FPP to form a thiol ether bond with farnesyl, coordinates directly to the active site zinc. On the basis of the X-ray structure of the active site and in particular the region of the three reactive elements, C1 of FPP, the active site Zn^{2+}, and the cysteine thiol of a CaaX-containing substrate, a systematic analysis of the roles of adjacent FPT amino acids in catalysis can be performed via the kinetic characterization of mutants. In this report, we describe the results from an analysis of eight FPT mutants within the active site. The selection of these mutants was based on their proximity to the three reactive elements as observed in the three-dimensional X-ray structure of the FPT−αHFP−CVIM complex. From steady-state kinetic characterizations, pre-steady-state kinetic analysis, and pH-dependent rate studies, we have identified several residues that appear to be important for catalytic activity, and thus, a FPT reaction mechanism is proposed.

MATERIALS AND METHODS

Materials. [1-^{3}H]FPP (21.5 Ci/mmol) was purchased from New England Nuclear Life Science Products (Boston, MA). Streptavidin-coated scintillation beads were obtained from Amersham (Arlington Heights, IL). Biotinylated KKSKTKCVIM was from Analytical Biotechnology Services (Boston, MA). Recombinant wild-type rat FPT with a 19-amino acid N-terminal His tag on the α-subunit was purified from *Escherichia coli* BL21(DE3)/pZWF02 cells as described elsewhere (*26*). *E. coli* strain BL21(DE3) was purchased from Novagen (Madison, WI). All restriction enzymes and Vent polymerase were obtained from New England Biolabs (Beverly, MA). Oligonucleotides were bought from Genosys (Woodlands, TX). Sodium dodecyl sulfate−polyacrylamide gel electrophoresis (SDS−PAGE) was performed with precast Tris-Glycine gels purchased from Bio-Rad (Hercules, CA). Unless specified, all other materials were purchased from Sigma (St. Louis, MO).

Preparation of FPT Mutants. Plasmid pZWF02, an expression vector that encodes the FPT α- and β-subunits in a tandem cistron (*26*), was used as a template for all mutagenesis experiments. Amino acid changes are abbreviated such that Y300Fβ indicates an FPT mutant in which the β-subunit residue tyrosine 300 has been changed to a phenylalanine. Most of the FPT mutants were prepared using a PCR overlap extension method (*27*). Oligonucleotide pairs that were used to introduce mutation in the forward and reverse directions are listed below, with the mutated nucleotides in boldface and underlined. Primers for H248Aβ are F-30 (5′-GGATGGAAGCC**GC**CGGTGGCTACAC-3′) and F-31 (antiparallel) (5′-GTGTAGCCACCG**GC**GGCTTCCATCC-3′). Primers for Y300Fβ are F-32 (5′-TGGACGGCTGCT**T**CTCCTTCTGGCA-3′) and F-33 (antiparallel) (5′-TGCCAGAAGGAG**A**AGCAGCCGTCCA-3′). Primers for Y200Fα are F-35 (5′-GATGCAAAGAATT**T**CCATGCCTGGCAG-3′) and F-36 (antiparallel) (5′-CTGCCAGGCATGG**A**AATTCTTTGCATC-3′). Primers for H201Aα are F-37 (5′-GCAAAGAATTAC**GC**TGCCTGGCAGCAT-3′) and F-38 (antiparallel) (5′-ATGCTGCCAGGCA**GC**GTAATTCTTTGC-3′). Primers for Y166Fα are F-41 (5′-GAACAGCCCAAAAACT**T**TCAAGTTTGGCACCAT-3′) and F-42 (antiparallel) (5′-ATGGTGCCAAACTTGA**A**AGTTTTTGGGCTGTTC-3′). Primers for Y166Aα are F-43 (5′-GAACAGCCCAAAAAC**GC**TCAAGTTTGGCACCAT-3′) and F-44 (antiparallel) (5′-ATGGTGCCAAACTTGA**GC**GTTTTTGGGCTGTTC-3′). Y361Fβ was constructed by replacing the *Pml*I−*Hin*dIII fragment of the β-subunit ORF of pZWF02 with a newly synthesized DNA fragment. The DNA carrying the amino acid change at Y361β was prepared via a PCR with the start primer F-34 (5′-AACCTGGCAAGTCACGTGACTTCT**T**CC-3′) and the end primer F-29 (antiparallel) (5′-CCCAAGCTTGGATCCTAGTCAGTGGCAGGATCTGAGGTCACC-3′). The F-29 primer had an additional *Bam*HI site (underlined) right after the stop codon for screening. K164Nα and a double mutant, Y300Fβ/H248Aβ, were prepared using a QuikChange site-directed mutagenesis kit (Stratagene, La Jolla, CA). The primers for K164Nα are F-45 (5′-GAGGAACAGCCCAA**T**AACTATCAAGTTTGGCAC-3′) and F-46 (antiparallel, 5′-GTGCCAAACTTGATAGTT**A**TTGGGCTGTTCCTC-3′). The double mutant was constructed using the Y300Fβ DNA as a template, and a primer pair of F-30 and F-31 to introduce the additional H248Aβ mutation. All mutated regions were sequenced to confirm the intended change. Resultant plasmids encoding FPT mutants were subcloned in *E. coli* DH5α,

and subsequently transformed into *E. coli* BL21(DE3) for protein production. All the expressed mutants contain the pZWF02-derived 19-amino acid N-terminal His tag on the α-subunit.

Mutant production and purification were performed as described for wild-type FPT (*26*). The final protein preparations were ca. 90% pure as judged by SDS−PAGE. The protein identities were confirmed by Western blotting using a BCIP/NBT kit (Kirkegaard & Perry Laboratories, Gaithersburg, MD) with an anti-α-subunit and an anti-β-subunit polyclonal antibody, as well as by N-terminal amino acid sequencing. The molecular weights of mutants were determined by MALDI mass spectroscopy with sinapinic acid as the matrix on a Voyager DE TOF mass spectrometer (PerSeptive Biosystem, Framingham, MA). Protein concentrations were determined either by the method of Bradford (*28*) using a Bio-Rad assay kit with bovine serum albumin (BSA) as a standard or by using the UV absorbance at 280 nm with a molar extinction coefficient of 1.53×10^5 M^{-1} cm^{-1}. Far-UV circular dichroism (CD) measurement of the purified mutants (0.07 mg/mL) was performed in a 10 mM sodium phosphate, 1 mM DTT, pH 7.4 buffer on a JASCO J-500C spectropolarimeter from 200 to 250 nm. Spectra were recorded at room temperature using a 0.1 cm path length cell and were the average of four to eight scans. A solvent spectrum was subtracted from each protein spectrum. Each protein spectrum was normalized on the basis of concentration determined from an UV absorbance spectrum.

Steady-State Kinetic Analysis. Steady-state kinetic parameters of the mutants were determined using a scintillation proximity assay (SPA) in a 96-well plate format as described for wild-type FPT (*26*). Briefly, an assay was initiated by the addition of purified enzyme (0.5−10 nM) to a mixture of a CaaX-containing peptide, biotinylated KKSKTKCVIM, and [1-^{3}H]FPP at 23 °C in a volume of 200 μL. The assay buffer consisted of 50 mM Tris (pH 7.7), 5 mM $MgCl_2$, 5 μM $ZnCl_2$, 0.01% Triton X-100, 0.2 mg/mL BSA, and 2 mM DTT. Concentrations of both substrates were set between $K_m/2$ and $10K_m$ when possible, and the extent of substrate consumption was limited to less than 10%. Aliquots of the reaction mixture (50 μL) were withdrawn over time and the reactions immediately quenched with 150 μL of buffer containing 5 mg/mL scintillation beads, 500 mM EDTA (pH 8.0), and 0.5% BSA. After incubation of the quenched mixture for 30 min, the radioactivity in the product was determined and used for the calculation of an initial velocity.

The Michaelis−Menten reaction rate equation for an ordered bi-bi mechanism with substrate inhibition is given by

$$V_i = (k_{cat}[E]_o[FPP][PEP])/([[FPP][PEP] + K_m^P[FPP] + (K_m^F[PEP] + K_m^P K_D^F)(1 + [PEP]/K_I)] \quad (1)$$

where k_{cat} is the enzyme turnover number, K_I is the substrate inhibition constant associated with the E·PEP complex, K_D is the dissociation constant for the E·FPP complex, and K_m^P and K_m^F are Michaelis constants for peptide and FPP, respectively, when the second substrate is at an infinite concentration (*34*). Due to the five kinetic parameters that have to be calculated simultaneously from eq 1 and the experimental design for calculating k_{cat} and K_m values, the initial velocities at various concentrations of two substrates that globally fitted to eq 1 resulted in K_D and K_I values with high degrees of uncertainty. Since the peptide concentrations that were used (25−500 nM) were significantly lower than the K_I of 1.3 μM (*26*), and using the assumption that the K_m^F is approximately equal to the K_D for FPP, then eq 1 can be simplified to eq 2 as described previously (*17*).

$$V_i = (k_{cat}[E]_o[FPP][PEP])/([FPP][PEP] + K_m^P[FPP] + K_m^F[PEP] + K_m^P K_m^F) \quad (2)$$

The initial velocities at various concentrations of two substrates were globally fitted to eq 2 for simultaneous calculation of k_{cat}, K_m^P, and K_m^F. The nonlinear least-squares fit of the data was performed using Sigma Plot (Jandel Scientific, San Rafael, CA). All the kinetic experiments were repeated at least three times.

Pre-Steady-State Kinetic Experiments. Pre-steady-state kinetic experiments with wild-type FPT and mutants K164Nα, H248Aβ, and Y300Fβ were performed using a procedure similar to that described for yeast FPT (*18*) on a KinTek RQF-3 Rapid Quench-Flow apparatus (State College, PA) equipped with a thermostatically controlled circulator (*29*). The sample and reaction loop volumes were measured to within 1% with a solution of [^{14}C]isopentenyl diphosphate (400 cpm/μL). Measurements were performed at 23 °C with a pre-equilibrated solution of FPT/[1-^{3}H]FPP in the first sample loop (24 μL) and biotinylated KKSKTKCVIM in the second loop (24 μL), with the buffer used for the steady-state kinetic analysis described above. Final sample concentrations after mixing were 0.5 μM enzyme, 5 μM [1-^{3}H]FPP (818 Ci/mol), and 5 μM biotinylated KKSKTKCVIM. Reactions were quenched with 200 μL of 0.2 M HCl at time intervals ranging from 0.1 to 600 s. The ejected liquid was collected in 13 mm × 70 mm glass tubes and placed on ice. A 150 μL portion was removed, spotted onto a phosphocellulose strip, and analyzed as described previously (*18*). Blank reactions were performed in separate Eppendorf tubes with the quench solution added to the pre-equilibrated FPT−FPP complex prior to the addition of the peptide substrate.

The amount of the farnesylated peptide (F-PEP), as determined using the phosphocellulose filter assay, was plotted versus time and fit to eq 3,

$$[F\text{-}PEP]_{obs} = [F\text{-}PEP] + [E{\cdot}F\text{-}PEP{\cdot}PP_i] = \alpha(1 - e^{-\beta t}) + \gamma t \quad (3)$$

in which α is an apparent burst amplitude, β is the reciprocal lifetime of the enzyme−product complex (E·F-PEP·PP_i), and γ is a steady-state rate. Nonlinear least-squares analysis of the data in estimating the kinetic parameters α, β, and γ was performed using the program KaleidaGraph (Synergy Software). In the experiments, the enzyme (0.5 μM) was pre-equilibrated with FPP (5 μM), and therefore, all FPT was assumed to be in the form of E·FPP. On the basis of a minimal kinetic mechanism of FPT as depicted in Scheme 1, the three parameters α, β, and γ can be redefined in eqs 4−7. The first-order rate constants for product formation and product release are k_3 and k_4, respectively,

Scheme 1: A Kinetic Model for FPT

$$E \cdot FPP \underset{k_{-2}}{\overset{k_2\ PEP}{\rightleftharpoons}} E \cdot FPP \cdot PEP \xrightarrow{k_3} E \cdot F\text{-}PEP \cdot PP_i \xrightarrow{k_4} \text{products}$$

while k' is an effective first-order rate constant for product formation.

$$\alpha = E[\mathrm{FPP}]_o\left(\frac{k'}{k' + k_4}\right)^2 \quad (4)$$

$$\beta = k' + k_4 \quad (5)$$

$$\gamma = E[\mathrm{FPP}]_o\left(\frac{k'k_4}{k' + k_4}\right) \quad (6)$$

$$k' = \frac{k_3[\mathrm{PEP}]}{(k_{-2} + k_3)/k_2 + [\mathrm{PEP}]} \quad (7)$$

The α, β, and γ values were estimated from the best fits of the data to eq 3. Rate constants k_3 and k_4 were calculated by substituting values for α, β, and γ into eqs 4−7.

pH−Rate Profiles. K_m and k_{cat} values of wild-type FPT and mutants K164Nα and Y300Fβ at pHs not equal to 7.7 were obtained using a universal buffer containing the following each at 20 mM: malic acid, 2-(*N*-morpholino)ethanesulfonic acid (MES), 4-(2-hydroxyethyl)-1-piperazineethanesulfonic acid (HEPES), and boric acid. The pH of the buffer was adjusted to 4.5, 5.5, 6.0, 6.5, 7.0, 7.5, 8.0, 8.5, 9.0, 9.5, and 10.5. Unless specified, all of the pH−rate studies were performed under the same assay conditions that were described for the steady-state kinetic analysis. Enzyme was preincubated in the appropriate pH buffer for 30 min at 23 °C prior to being mixed with the substrates. For the series of experiments in which the FPP concentration was varied (from 5 to 200 nM), the concentration of biotinylated KKSKTKCVIM was fixed at 300 nM. The apparent V_{max}^F and K_m^F values (for FPP) at different pHs were determined from the Michaelis−Menten equation, and were applied to eqs 8 and 9 for calculating pK_a (acidic side) and pK_b (basic side) values of bell-shaped pH−rate curves.

$$V_{max}' = V_{max}/[1 + 10^{(\mathrm{pH}-\mathrm{p}K_{a2})} + 10^{(\mathrm{p}K_{b2}-\mathrm{pH})}] \quad (8)$$

$$V_{max}'/K_m' = (V_{max}/K_m)/[1 + 10^{(\mathrm{pH}-\mathrm{p}K_{a1})} + 10^{(\mathrm{p}K_{b1}-\mathrm{pH})}] \quad (9)$$

For the series of experiments with varied peptide concentrations (from 25 to 500 nM), the FPP concentration was fixed at 100 nM, and V_{max}^P and K_m^P for the peptide substrate were determined in a similar manner. The enzyme concentrations used in the assays were 5 nM for wild-type FPT, 6 nM for Y300Fβ, and 12 nM for K164Nα. All of the experiments were repeated at least three times. The nonlinear least-squares fit of the data for calculation of apparent p*K* values was performed using the program KaleidaGraph (Synergy Software). Equations 8 and 9 were derived for a simple Michaelis−Menten reaction. Subscript letters denote the side of the bell-shaped pH−rate curve from which the apparent p*K* values are calculated, acidic (pK_a) or basic (pK_b). The subscript numbers indicate the equation from which the p*K* values are derived, eq 8 (pK_2) or eq 9 (pK_1).

The stability of FPT activity was investigated over a pH range from 4.5 to 10.5 to validate the pH−rate studies. Wild-type FPT was preincubated in the universal buffer at an appropriate pH for 30 min at 23 °C, and was subsequently diluted 10-fold in the buffer for the steady-state kinetic analysis (pH 7.7). After incubation for 15 min, FPT activity was measured by the SPA assay. There was no significant change in the activity (<20%) of FPT incubated between pH 4.5 and 9.5, whereas the enzyme incubated at pH 10.5 retained about 65% of the maximal activity. Therefore, the pH range that was used is suitable for pH−rate studies.

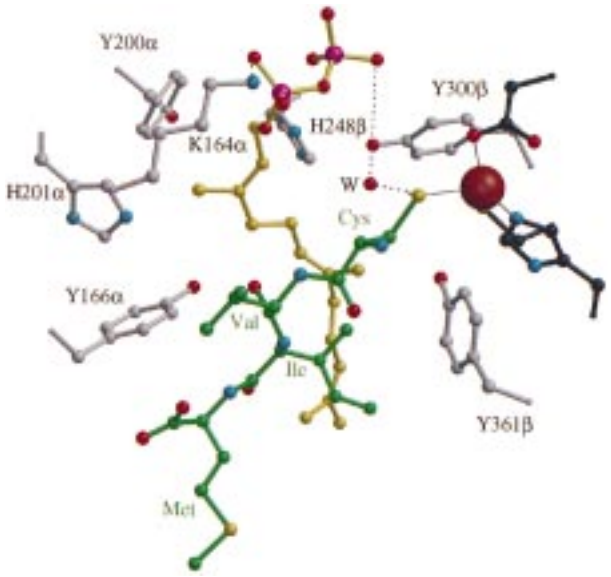

FIGURE 1: Schematic view of seven amino acid residues in the rat FPT active site with a bound CVIM peptide, acetyl-Cys-Val-Ile-seleno Met-COOH, and farnesyl diphosphate (FPP). This structure was adapted from the reported three-dimensional crystal structure (*24*) with FPP replacing αHFP, and displayed using Insight II (Biosym Technologies, San Diego, CA). The solid sphere highlights the endogenous zinc ion in the active site. CVIM, FPP, and the side chains of amino acid residues K164α, Y166α, Y200α, H201α, H248β, Y300β, and Y361β are shown in ball-and-stick format. A well-defined water molecule (W) between Y300β and the cysteine thiol is shown as a red sphere. Hydrogen bonds are shown as dashed lines. The backbone of CVIM is green and the backbone of FPP yellow. The mutated residue side chains are gray and the zinc ligands black. Oxygen is red, nitrogen blue, phosphorus pink, sulfur yellow, and zinc orange.

RESULTS

Mutagenesis of FPT Active Site Residues. The three-dimensional structure of rat FPT complexed with a CVIM peptide and αHFP (*24*) shows that C1 of the farnesyl group, the catalytic Zn^{2+}, and the cysteine thiol of a CaaX-containing substrate are in close proximity to each other. A similar conclusion is reached for a three-dimensional model containing FPT−CVIM and FPP which is generated by removing αHFP and superimposing an independent FPT−FPP structure. The model complex composed of the FPT−FPP−CVIM structure shown in Figure 1 will be referenced throughout the text.

To determine which amino acid residues were important in catalysis, we mutated four amino acid residues (K164α, Y300β, H248β, and Y361β) that are in close proximity to the C1 of FPP and the cysteine thiol, as well as three residues (Y166α, Y200α, and H201α) which contribute to the first isoprene (C1−C5) binding pocket of FPP. Mutants were constructed such that tyrosine residues were changed to

Table 1: Steady-State Kinetic Parameters of FPT and Mutants[a]

enzyme	k_{cat} (min^{-1})	K_M^F (nM)	K_M^P (nM)	$k_{cat}/K_M^F K_M^P$ (M^{-2} s^{-1})	relative activity
wild-type FPT	0.54 ± 0.05	14 ± 1	63 ± 10	(1.0 ± 0.3) × 10^{13}	100
K164Nα	0.094 ± 0.010	22 ± 2	45 ± 8	(1.6 ± 0.6) × 10^{12}	16 ± 6
Y166Fα	0.65 ± 0.02	18 ± 4	25 ± 6	(2.4 ± 1.2) × 10^{13}	240 ± 120
Y166Aα	0.015 ± 0.001	34 ± 6	104 ± 5	(7.1 ± 2.1) × 10^{10}	0.71 ± 0.21
Y200Fα	0.75 ± 0.12	990 ± 250	114 ± 21	(1.1 ± 0.6) × 10^{11}	1.1 ± 0.6
H201Aα	0.34 ± 0.02	29 ± 3	133 ± 16	(1.5 ± 0.4) × 10^{12}	15 ± 4
H248Aβ	0.54 ± 0.05	87 ± 27	40 ± 6	(2.7 ± 1.4) × 10^{12}	27 ± 14
Y300Fβ	0.15 ± 0.01	17 ± 1	103 ± 8	(1.5 ± 0.3) × 10^{12}	15 ± 3
Y361Fβ	1.3 ± 0.1	27 ± 2	61 ± 14	(1.3 ± 0.5) × 10^{13}	130 ± 50
Y300Fβ/H248Aβ	0.033 ± 0.001	29 ± 2	52 ± 14	(3.7 ± 0.4) × 10^{11}	3.7 ± 0.4

[a] The kinetic parameters are the average of at least two sets of data.

phenylalanines or alanines, histidines were substituted with alanines, and a lysine was replaced by an asparagine. These substitutions were designed to remove the potentially reactive groups and to minimize the mutagenic impact on protein secondary structure. Eight single mutants, K164Nα, Y166Fα, Y166Aα, Y200Fα, H201Aα, H248Aβ, Y300Fβ, and Y361Fβ, and one double mutant, Y300Fβ/H248Aβ, were constructed in *E. coli*. All of the mutants were expressed at levels similar to that of the wild-type enzyme, and purified to ca. 90% homogeneity through a two-step chromatography procedure as described for wild-type FPT (*26*). There was no obvious change in behavior for any of the mutants during the purification. Far-UV CD analysis was performed for all of the purified mutants. On the basis of the shape and magnitude of the far-UV CD spectra, there was no significant change in the secondary structure for any of the mutants.

Steady-State Kinetic Analysis. The steady-state kinetic properties of the mutants were examined at 23 °C using the SPA assay as described in Materials and Methods. Michaelis constants for FPP (K_m^F) and biotinylated KKSKTKCVIM (K_m^P) and the enzyme turnover number (k_{cat}) were determined for each mutant protein and are summarized in Table 1. The catalytic efficiency of each species, as measured by a second-order rate constant, $k_{cat}/K_m^F K_m^P$, is also reported along with the relative activity of each mutant compared to wild-type FPT which was normalized to 100. His-tagged wild-type FPT has a k_{cat} of 0.54 min^{-1}, and Michaelis constants for FPP and the peptide are 14 and 63 nM, respectively (Table 1). Five of the eight single mutants (Y166Fα, Y200Fα, H201Aα, H248Aβ, and Y361Fβ) were active with k_{cat} values comparable to or higher than that of the wild-type enzyme.

Residue Y166α undergoes a relatively large conformational change upon binding FPP (*24*). Compared to the wild-type enzyme, the Y166Fα mutant had a slightly higher k_{cat} value (0.65 min^{-1}) and a similar K_m^F value (18 nM). A lower Michaelis constant for the peptide substrate (K_m^P = 25 nM) contributed to a higher catalytic efficiency for the mutant than for the wild-type enzyme. These results suggest that the hydroxyl group on Y166α is not critical for either catalytic activity or substrate binding. Y166α was also mutated to an alanine, and the kinetics of this mutant were significantly different from those of Y166Fα with larger values for K_m^P (104 nM) and K_m^F (34 nM). In addition, the k_{cat} value was only 0.015 min^{-1} which was one of the lowest values of all the mutants that were examined (Table 1). It appears that the aromatic ring of tyrosine is important for substrate binding. Although k_{cat} was decreased significantly, it is likely that a conformational change in the active site resulting from the Y166Aα substitution (Figure 2) affects catalysis rather than Y166α being directly important in the reaction (see the Discussion).

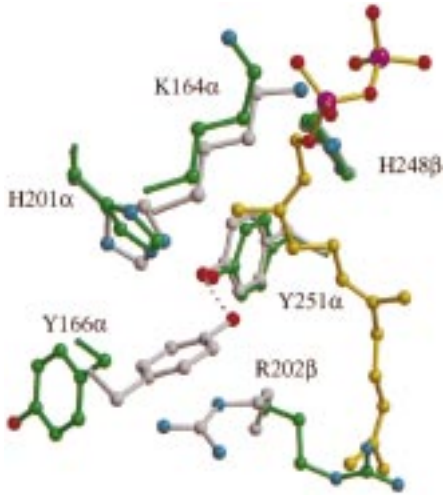

FIGURE 2: Schematic view of Y166α and interacting residues Y251β, R202β, and H201α before and after the binding of the CVIM peptide and FPP in the FPT active site. The residue side chains for the unliganded conformation are gray. Those for the liganded conformation are green. The backbone of FPP is yellow, oxygen red, nitrogen blue, and phosphorus pink.

Mutants Y200Fα, H201Aα, H248Aβ, and Y361Fβ all exhibited elevated K_m^F values, especially Y200Fα in which the K_m^F value (990 nM) was 71 times higher than that of wild-type FPT (Table 1). On the basis of the crystal structure of FPT (*24*), Y200α forms a hydrogen bond with the backbone amide of G241β, and contributes to a hydrophobic binding pocket for the first isoprene unit of FPP (Figure 1). Removal of the tyrosyl hydroxyl of Y200α would disrupt the hydrogen bond and lead to a rearrangement of both residues in the isoprene-binding pocket, resulting in less optimal binding for FPP. Compared to the wild-type enzyme, mutant H201Aα had both K_m^F and K_m^P values increased by 2-fold. The k_{cat} value was decreased 1.6-fold, which may be caused by the loss of an edge-to-face interaction with Y166α (see the Discussion). The magnitude of the decrease suggests that the imidazole is not critical for catalysis. The decrease in substrate affinity is consistent with structural analysis, indicating that an alanine substitution of H201α would lead to the loss of van der Waals interactions with the first isoprene unit of FPP and the edge-to-face interaction with Y166α (*24*). In addition, the loss of the water that mediates the hydrogen bond between H201α and the CVIM backbone is also likely to contribute to a decrease in the peptide affinity (*24*).

Residue H248β forms a 2.7 Å hydrogen bond with the bridge oxygen between C1 and α phosphate of FPP, and is within 3.6 Å of C1 (Figure 1). Replacement of this residue with an alanine (H248Aβ) increased the K_m^F by 6-fold, which is consistent with its role in binding to the diphosphate. Interestingly, H248Aβ had the same k_{cat} value as the wild-type enzyme. Although it is the residue closest to C1 of FPP, H248β does not appear to contribute directly to catalysis. Similar kinetic results were observed for the H248Aβ mutant in human FPT (*30*). Y361β is located in the vicinity of both the cysteine thiol and the zinc ion and makes van der Waals contact with the isoleucine residue of the peptide substrate (Figure 1). Compared to the wild-type enzyme, Y361Fβ had a similar K_m^P and only a 2-fold higher K_m^F. In addition, Y361Fβ was the only mutant that had a k_{cat} (1.3 min^{-1}) significantly higher than that of the wild-type enzyme, which when combined with the K_m values, resulted in a fully active mutant (Table 1). The fact that the tyrosyl hydroxyl is not important for catalysis is consistent with the fact that Y361β is not conserved between FPT and GGPT I, in which this residue is a leucine. A recent report suggested that this residue in yeast FPT (Y362β) may contribute to the enzyme's substrate specificity (*31*).

Two single mutants, K164Nα and Y300Fβ, were the most interesting because of their proximity to the reaction site and lower enzyme turnover rates. K164α and Y300β are conserved among all known FPT and GGPT I species, and both form hydrogen bonds with the FPP diphosphate (Figure 1). The mutants K164Nα and Y300Fβ had k_{cat} values of 0.094 and 0.15 min^{-1}, respectively, which are 5.7- and 3.6-fold lower than that of the wild-type enzyme, respectively (Table 1). These results are similar to values previously reported for rat and human FPT mutants (*30*, *32*). Pre-steady-state kinetic studies have indicated that the k_{cat} from steady-state kinetic studies only reflects the rate-limiting step, which is product release (*17*). Therefore, a small change in k_{cat} could mask a more profound change in the rate constant for the actual chemical step. For this reason, additional pre-steady-state kinetic studies were performed with these mutants (see below).

The double mutant, Y300Fβ/H248Aβ, was constructed because of the proximity of each residue to the three reactive elements and the kinetic results for each single mutant. The k_{cat} value (0.033 min^{-1}) of this double mutant is 16-fold lower than that of the wild-type enzyme. The K_m^F of the mutant was 2 times higher than that of the wild-type enzyme, and the K_m^P was essentially the same. The values of these kinetic parameters did not exhibit a simple additive effect from the two single mutants Y300Fβ and H248Aβ. The double mutant had a lower K_m^F value than H248Aβ and a lower K_m^P value than Y300Fβ, while the k_{cat} value for Y300Fβ/H248Aβ was 4.5-fold lower than that for Y300Fβ. These results suggest that either H248β contributes to the catalysis once Y300β is mutated or the two combined amino acid substitutions result in a further disruption of the enzymatic activity by another mechanism. Further investigation is necessary to understand the cause of the lower k_{cat} value.

Pre-Steady-State Kinetic Experiments. Pre-steady-state kinetic studies were conducted to measure the transient- and steady-state rates of the reaction for the *E. coli*-derived rat FPT and three mutants, K164Nα, H248Aβ, and Y300Fβ. Rapid quench techniques were employed for this measurement using a procedure previously developed for yeast FPT (*18*). Like the Sf9 cell-derived rat FPT (*17*) and the yeast enzyme (*18*), our *E. coli*-derived rat FPT exhibited biphasic kinetics consisting of a rapid exponential phase followed by a slower linear steady-state phase (Figure 3). On the basis of a minimal kinetic model of FPT as illustrated in Scheme 1, the exponential phase could originate from a fast single turnover of the enzyme, either k_2 or k_3, whereas the steady-state phase reflects the rate-limiting product-releasing step, k_4. In the reported rapid quench experiments using Sf9-derived rat FPT (*17*), the rate constant derived from the exponential phase was found to be peptide concentration-dependent and, therefore, was proposed to be the second-order rate constant k_2 in Scheme 1. As a result, the exponential phase would correspond to the formation of the enzyme-bound product FPT·F-PEP·PP_i ternary complex from FPT·FPP and the peptide substrate PEP. However, similar experiments with yeast FPT demonstrated that the rate constant from the exponential phase was first-order and corresponded to the conversion of the ternary complex to products, k_3 (*18*). To assess which step the exponential phase represented in our experiments, rapid quench experiments were performed with peptide substrate concentrations set at 5, 10, and 15 μM. When wild-type FPT was used, the rates calculated from the exponential phase (burst phase) varied only slightly with increasing peptide concentrations, and did not exhibit a linear dependence on peptide concentrations (data not shown). In addition, for the Y300Fβ mutant, the rates deduced from the exponential phase were clearly independent of peptide concentration (Figure 4). From these results, it can be inferred that the rate constant obtained from the exponential phase represents the chemical step, k_3, in the reaction.

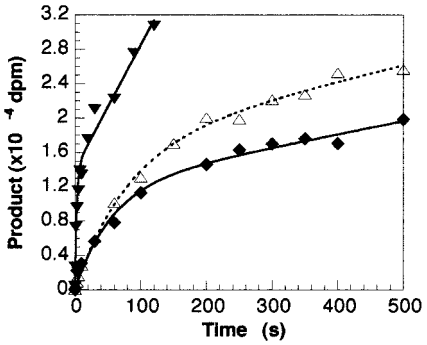

FIGURE 3: Time course of the rapid quench experiments with wild-type FPT (▼) and K164Nα (△) and Y300Fβ (◆) mutants. The data for the H248Aβ mutant are not shown here. Enzyme (0.5 μM) was mixed with 5 μM [1-^{3}H]FPP and 5 μM biotinylated KKSKT-KCVIM (final concentration) at 23 °C in a KinTek RQF-3 Rapid Quench-Flow apparatus to initiate a reaction. Reactions were stopped with 0.2 M HCl at time intervals ranging from 0.1 to 600 s. The amount of product generated was determined by a phosphocellulose filter assay. Data were fitted to eq 3 for the calculation of kinetic parameters. The lines represent the calculated fit with one set of data for each enzyme species.

The results from the rapid quench experiments using wild-type FPT and a peptide concentration of 5 μM were applied to eq 3 and yielded the following kinetic parameters: $\alpha = 0.32 \pm 0.02$ μM, $\beta = 29 \pm 6$ min^{-1}, and $\gamma = 0.20 \pm 0.02$ μM min^{-1}. Since the experiment was conducted at a high peptide substrate concentration, k' in eq 7 should be approximately equal to k_3. With this approximation, applica-

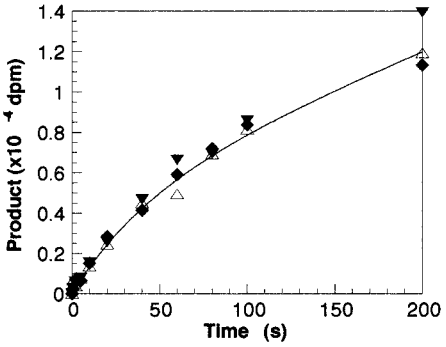

FIGURE 4: Rapid quench experiments with the Y300Fβ mutant at various peptide substrate concentrations. Enzyme (0.5 μM) was mixed with 5 μM [1-^{3}H]FPP and biotinylated KKSKTKCVIM to initiate a reaction. The peptide concentration was set at 5 (▼), 10 (△), and 15 μM (◆). Reactions were quenched with 0.2 M HCl at time intervals ranging from 0.1 to 200 s. The amount of product generated was determined by a phosphocellulose filter assay, and analyzed by fitting to eq 3. For the clarity of the graphic, only the data with 5 μM peptide substrate were fit to eq 3.

tion of eqs 4−7, and the propagation of errors formula, k_3 and k_4 values were determined to be 29 ± 6 and 0.60 ± 0.09 min^{-1}, respectively (Table 2). Notably, k_4 was in good agreement with the k_{cat} value (0.54 min^{-1}) from the steady-state kinetics. These results suggest that for rat FPT, the chemical step is 48 times faster than product release.

Similar rapid quench experiments were conducted with the three single mutants K164Nα, H248Aβ, and Y300Fβ (Figure 3). The results are summarized in Table 2. Mutant H248Aβ had a kinetic profile similar to that of the wild-type enzyme with both k_3 and k_4 values in good agreement. This result is consistent with the conclusion from the steady-state kinetic analysis that residue H248β is not critical for catalysis. In contrast, rapid quench experiments with K164Nα and Y300Fβ yielded quite different pre-steady-state kinetic profiles. Compared to values for the wild-type enzyme, k_3 for K164Nα decreased 41-fold to 0.70 min^{-1} and k_4 decreased 9-fold to 0.063 min^{-1}. Similarly, k_3 and k_4 for Y300Fβ were reduced by 30- and 10-fold, respectively. Clearly, the side chains of residues K164α and Y300β play an important role in both the catalytic step and product release.

pH Dependence of V_{max} and V_{max}/K_m. To further explore the kinetic properties of the wild-type enzyme as well as those of the K164Nα and Y300Fβ mutants, the enzymatic activities were examined with respect to pH. Although FPT catalyzes a sequentially ordered bi-bi reaction (*17*), it can be treated as a simple Michaelis−Menten enzyme when one of the substrates is fixed at a high concentration. Using this approach, eqs 8 and 9 can be applied for the determination of pK values of the apparent titratable groups that are important for enzyme activity.

For wild-type FPT, the pH dependencies of V_{max}^F and $(V_{max}/K_m)^F$ were examined using varying FPP concentrations and a fixed peptide concentration over a pH range from 4.5 to 10.5. The $(V_{max}/K_m)^F$−pH profile was not bell-shaped (data not shown), while the V_{max}^F−pH plot was (Figure 5A). The fit of the pH−V_{max}^F profile to eq 8 yielded inflection points with an apparent pK_{a2} of 7.0 ± 0.1 on the acidic side and an apparent pK_{b2} of 9.3 ± 0.2 on the basic side (Table 3). The pH-dependent V_{max}^P and $(V_{max}/K_m)^P$ for varying peptide concentrations were also determined for the pH range between 4.5 and 10.5. The pH−$(V_{max}/K_m)^P$ profile was bell-shaped with a pK_{a1} of 6.0 ± 0.2 and a pK_{b1} of 9.1 ± 0.1 (Figure 5B). Interestingly, the variation of V_{max}^P with pH was only half-bell-shaped with a pK_{a2} of 7.0 ± 0.2.

The pH dependence of the Y300Fβ activity was examined under conditions similar to those of the wild-type enzyme. The pH−$(V_{max}/K_m)^F$ curve was half-bell-shaped with an apparent pK_{a1} of 5.8 ± 0.4. The pH−V_{max}^F plot exhibited a bell-shaped relationship with a pK_{a2} of 6.0 ± 0.1 on the acidic side and an apparent pK_{b2} of 9.4 ± 0.1 on the basic side (Figure 5A). With varying concentrations of peptide, the pH−$(V_{max}/K_m)^P$ curve was bell-shaped and had a pK_{a1} of 6.2 ± 0.3 and a pK_{b1} of 8.1 ± 0.3 (Figure 5B). The pH−V_{max}^P profile with variations in the peptide concentration was also bell-shaped with pK values similar to those acquired for varying concentrations of FPP (Table 3). These results indicate that the mutant Y300Fβ has a pH−rate profile that is different from that of the wild-type enzyme and confirm that the hydroxyl group is important for the activity of the enzyme. Similarly, pH−rate studies with K164Nα were also performed, and the results are summarized in Table 3. Overall, the apparent pK values for K164Nα were similar to those of the wild-type enzyme, except that the pK_{a1} values from pH−V_{max}/K_m experiments decreased 0.7 pH unit to 5.3.

DISCUSSION

FPT is an important therapeutic target with the potential to treat several oncogenic Ras-related cancers. To elucidate the enzymatic reaction mechanism, we have determined the three-dimensional X-ray structure of FPT complexed with substrate analogues (*24*). On the basis of this structure, we undertook a systematic mutagenesis of the putative catalytic residues in the active site and conducted steady-state and pre-steady-state kinetic studies with these mutants. From the steady-state analysis, it is clear that residues Y200α, H201α, H248β, and Y361β mainly contribute to substrate binding and not catalysis.

Residue Y166α undergoes a large conformational change upon substrate binding (*24*). From the unliganded state to the liganded complex, its side chain undergoes an approximate 110° rotation about χ_1 in forming a hydrogen bond with the Y251β hydroxyl, a cation−π interaction with the guanidino group of R202β, and an edge-to-face interaction with the H201α imidazole (Figure 2). In addition, Y166α also forms van der Waals contacts with the first isoprene unit of FPP and the CVIM peptide valine isopropyl group (Figure 1). Our steady-state kinetic results for the conservative mutation Y166Fα suggest that the hydrogen bond between Y166α and Y251β is not critical for enzyme activity, contrary to a report using a crude lysate of this mutant (*32*). This result suggests that the interactions between Y166α and the other adjacent molecules are retained, and are sufficient to keep Y166Fα in an orientation that is optimal for interacting with the substrates. The fact that the hydrogen bond between Y166α and Y251β is not critical is consistent with the observation that Y251β is not conserved between FPT and GGPT I; this residue is a serine in human GGPT I. The importance of the cation−π and edge-to-face interactions between Y166α, R202β, and H201α becomes apparent from the kinetic analysis of the Y166Aα mutant. Cation−π interactions have been suggested to be important in the

Table 2: Data from Rapid Quench Experiments with Wild-Type FPT and Its Mutants

enzyme	α (μM)	β (min^{-1})	γ ($\mu M\ min^{-1}$)	k_3 (min^{-1})	k_4 (min^{-1})
wild-type FPT[a]	0.32 ± 0.02	29 ± 6	0.20 ± 0.02	29 ± 6	0.60 ± 0.09
K164Nα	0.38 ± 0.03	0.76 ± 0.11	0.026 ± 0.005	0.70 ± 0.12	0.063 ± 0.024
H248Aβ	0.18 ± 0.01	27 ± 8	0.096 ± 0.012	27 ± 8	0.53 ± 0.09
Y300Fβ	0.28 ± 0.03	1.1 ± 0.2	0.020 ± 0.004	0.96 ± 0.19	0.066 ± 0.019

[a] Average of two sets of data.

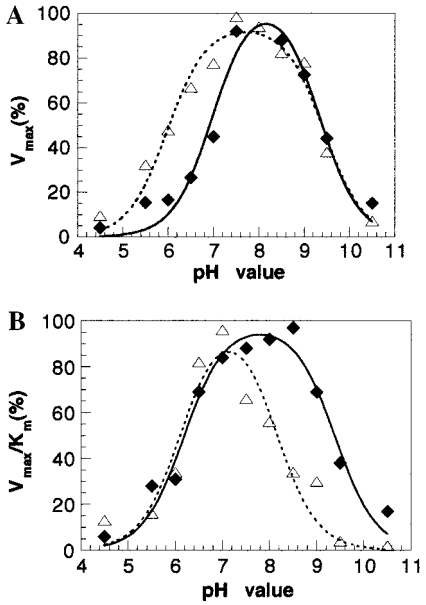

FIGURE 5: pH−rate profiles of wild-type FPT (◆) and the Y300Fβ mutant (△). All experiments were conducted using a SPA assay with the universal buffer as described in Materials and Methods. Experiments were repeated at least twice to ensure the consistency of the results. The relative activities of wild-type FPT and Y300Fβ at variant pH values are normalized to the highest activity (100%) for comparison. (A) pH−V_{max} profiles obtained with varying FPP concentrations (from 5 to 200 nM). The solid line (wild-type) and the dashed line (Y300Fβ) represent the best fits of the data to eq 8. (B) pH−V_{max}/K_m profiles obtained with varying peptide substrate concentrations (from 25 to 500 nM). The solid line (wild-type) and the dashed line (Y300Fβ) represent the best fits of the data to eq 9.

Table 3: pK Values of Wild-Type FPT and Its Mutants Obtained from pH−Rate Profiles

	V_{max}/K_m		V_{max}	
species/conditions	pK_{a1}	pK_{b1}	pK_{a2}	pK_{b2}
wild-type FPT				
varied FPP	−[a]	−[a]	7.0 ± 0.1	9.3 ± 0.2
varied peptide	6.0 ± 0.2	9.1 ± 0.1	7.0 ± 0.2	−[a]
K164Nα				
varied FPP	5.3 ± 0.2	9.3 ± 0.2	6.8 ± 0.2	9.4 ± 0.2
varied peptide	5.3 ± 0.2	9.6 ± 0.2	6.9 ± 0.1	9.5 ± 0.1
Y300Fβ				
varied FPP	5.8 ± 0.4	−[a]	6.0 ± 0.1	9.4 ± 0.1
varied peptide	6.2 ± 0.3	8.1 ± 0.3	5.7 ± 0.1	9.4 ± 0.1

[a] No bell-shaped pH−rate plot was obtained for the pK determination.

stabilization of active site conformations in biological macromolecules (*33*). The Y166Aα mutant experiences a 36-fold decrease in its k_{cat} value and a 2-fold decrease in its substrate affinity. Figure 2 shows that the conformations of Y166α, R202β, and H201α in the absence of substrates are significantly different from the liganded conformation. It is likely that the ligand-induced conformational changes of these residues are disrupted in the Y166Aα mutant due to the loss of the R202β's cation−π and H201α's edge-to-face interactions. The importance of the R202β's cation−π interaction is also reflected in the kinetic studies of the R202Aβ mutant whose K_m for peptide was reported to be increased by 500-fold and k_{cat} decreased by 2-fold (*30*). The conformational changes may be especially important since Y166α is located at the start of helix 5α and only two residues from the catalytically important residue K164α. The 36-fold decrease in k_{cat} for Y166Aα is likely to result from the conformational changes induced within the active site, rather than from the loss of a catalytically important tyrosine residue.

We have performed steady-state kinetic analysis on FPT mutants with substitutions at K164α, H248β, and Y300β, residues that are part of the binding pocket of the diphosphate moiety of FPP. R291β and K294β are the only other amino acid residues that bind directly to the diphosphate moiety (*24*). Substitutions of R291β and K294β with alanine have been reported to result in higher k_{cat} values and larger Michaelis constants for both substrates (*30*), suggesting that these residues are more important for substrate binding than for catalysis.

Kinetic analysis using our *E. coli*-derived rat Y300Fβ resulted in a k_{cat} value that was only 3.6-fold slower than that of the wild-type enzyme. A similar decrease in k_{cat} was observed for a human Y300βF mutant (*30*), while a 140-fold decrease was observed for a similar yeast mutant (*34*). In the rat and human mutants, the small decrease in k_{cat} may not reflect the real changes in the chemical step (k_3 in Scheme 1), since the rate-limiting step is product release. In the yeast enzyme, the rate of product release is only 3 times slower than the rate of the chemical step, and thus, the observed 140-fold decrease in k_{cat} should reflect a real decrease in k_3.

To probe the functions of Y300β and K164α in catalysis, we conducted the pre-steady-state kinetic measurements for the wild-type and mutant enzymes using rapid quench procedures. Previous pre-steady-state kinetic studies using stopped-flow techniques with a biotinylated GLPCVVM as the peptide substrate and a Sf9-derived rat FPT (*17*) determined that the rate constant for formation of the enzyme-bound product FPT·F-PEP, k_2, was $2.2 \times 10^5\ M^{-1}\ s^{-1}$ at 25 °C. In this same experiment, product release was identified as the rate-limiting step of the reaction. Rapid quench studies using our *E. coli*-derived rat FPT and a human K-Ras-4b peptide substrate (biotinylated KKSKTKCVIM) indicated that the rate constant for the conversion of the ternary complex to products, k_3, was 29 min^{-1} at 23 °C, while that of the product-releasing step was only 0.6 min^{-1}. If we assume that different enzyme sources and peptide substrates have a minimal effect on the rate constants k_2 and k_3, the rate constant for the formation of the ternary complex, k_2, would be 2.3 times faster than that of the chemical step, k_3,

at a peptide concentration of 5 μM. This approximation is consistent with our results showing that the exponential phase rate is not dependent on peptide concentration, thus indicating that the chemical step is slower than the formation of the ternary complex. The previously reported stopped-flow transient kinetic experiments detected the fluorescence changes induced from conformational transformations, whereas our rapid quench technique directly measures the rate of formation of products. These two methods determine the tandem rate constants, k_2 and k_3, and are complementary in elucidating FPT transient kinetics. The rapid quench results for FPT mutants K164Nα and Y300Fβ indicated that the k_3 and k_4 values were significantly reduced, suggesting that they are important for both catalysis and product release.

A comparison of pH−rate profiles between the wild-type and mutant proteins provides supporting evidence for the role of specific residues in the catalytic mechanism. p*K* values were obtained for wild-type FPT and Y300Fβ and K164Nα mutants (Table 3). The data for the variation of FPP or peptide concentrations are similar, indicating that the pH profiles are independent of the substrate whose concentration was varied. For wild-type FPT, the basic p*K* values deduced from pH−V_{max}/K_m or pH−V_{max} profiles are similar (pK_{b1} and pK_{b2}) and likely contributed by the same titratable group, while the acidic p*K*s are different (pK_{a1} and pK_{a2}) and represent different ionizable groups. The pH−rate profiles of wild-type FPT reveal three titratable groups, two acidic groups with pK_{a1} and pK_{a2} values of 6.0 and 7.0, respectively, and one basic group with a pK_b of 9.1−9.3. Replacement of Y300β with phenylalanine resulted in a shift of pK_{a2} (V_{max}−pH plot) from 7.0 to 6.0 and a change in pK_{b1} (V_{max}/K_m−pH plot) from 9.1 to 8.1 (Table 3). Therefore, residue Y300β contributes to the observed pK_{a2} of 7.0 and pK_{b1} of 9.1. The apparent pK_{a2} value of 7.0 is similar to that of catalytic tyrosines in π-class glutathione transferase and 3α-hydroxysteroid dehydrogenase (pK_a = 7.0−7.5) (*35*, *36*). The pH−rate profiles of wild-type FPT and Y300Fβ are consistent with Y300β functioning as a general acid−base in the reaction. The p*K* values for mutant K164Nα were altered by a 0.7 pH unit shift of the pK_{a1} from 6.0 to 5.3. This result provides additional evidence that K164α may be directly involved in the reaction, perhaps as a general acid. Since the observed p*K* values are the macroscopic products of pH−rate profiles, further spectroscopic titration experiments are necessary to determine the intrinsic p*K* values of the Y300β and K164α side chains.

There are several classes of enzymes that catalyze the alkylation of an activated thiol group in a manner similar to that of FPT, including glutathione transferase, methionine synthase, and the *E. coli* Ada protein (*37*). Among these, the zinc-dependent methionine synthase and the Ada protein are similar to FPT in utilizing an endogenous zinc to activate a cysteine/homocysteine thiol for a direct displacement reaction (*38*, *39*). Like FPT, isoprenoid synthases and transferases also use prenyl diphosphates as substrates (*40*, *41*). These enzymes catalyze prenyl cyclization and transformation through carbocation intermediates (*42*). In these reactions, a bound Mg^{2+} polarizes and activates the diphosphate moiety as a leaving group. As a result, an initial carbocationic intermediate is generated. Linear free energy correlations using a series of fluoro-substituted FPP analogues indicated that yeast FPT catalyzed an electrophilic

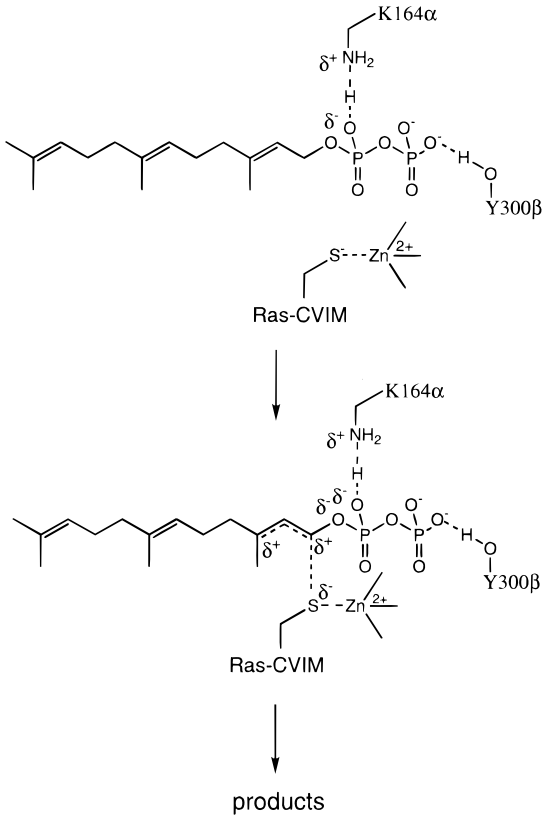

FIGURE 6: Proposed FPT reaction mechanism with residues K164α and Y300β playing important roles in enhancing the reactivity of the diphosphate moiety of FPP as a leaving group. The associative electrophilic intermediate is based on a previous study (*20*).

alkylation of the cysteine residue with substantial development of positive charge in the farnesyl moiety during the reaction (*20*). However, quantitative comparisons showed that the magnitude of positive charge that developed was significantly lower than that of the FPP synthase. Therefore, these results suggest the FPT-catalyzed reaction proceeds through an associative mechanism with a "late" or "exploded" transition state as shown in Figure 6 (*20*, *43*). An associative mechanism is also consistent with recent kinetic isotope experiments in which the α-secondary isotope effect using [1-$^2H_2$]FPP had a k_H/k_D ratio of close to unity (*44*). In addition, such a transition state will proceed with inversion of configuration at C1 of FPP as observed in NMR studies of the farnesylation reaction catalyzed by human FPT (*23*). An alternative to the associative transition state would be a more electrophilic one similar to the FPP synthase, proceeding through the ionization, condensation, and elimination steps; however, there would have to be some selective stabilization of the allylic cation that compresses the observed rates seen for the fluoro-FPP substrates.

Structural analysis indicates that residue K164α is located 2.8 Å from the α-phosphate oxygen (Figure 1). The proximity of this residue suggests that it should be able to donate a proton to the phosphate oxygen to enhance the reactivity of the diphosphate as a leaving group. Another potential general acid is Y300β which is 2.6 Å from the β-phosphate oxygens (Figure 1). This residue may also promote the reaction by hydrogen bonding to the leaving group. These proposals are consistent with the pH−rate studies which suggest that both K164α and Y300β may act as general acids. There are precedents for phosphate oxygens

acting as a general base to accept donated protons in enzymatic reactions. For example, in the D-Ala-D-Ala ligase reaction, the phosphate oxygen of the D-Ala phosphate intermediate is believed to act as a general base in abstracting a proton from the amino group of a second substrate, promoting a direct nucleophilic displacement (*45*). In farnesyl diphosphate synthase, a diphosphate-bound arginine is thought to enhance the reactivity of the leaving group (*46*).

FPT catalyzes a sequentially ordered reaction with FPP binding first to the enzyme active site, followed by the CaaX protein substrate. The structure of the FPT−FPP−CVIM complex shows that Y300β interacts with a water molecule that binds to the zinc-bound cysteine thiol through a hydrogen bond (Figure 1). If Y300β participates in the catalysis as a general acid, as shown in Figure 6, then the deprotonated Y300β tyrosyl could potentially act as a base that deprotonates the incoming cysteine thiol through the water hydrogen bond network. Interestingly, in the ζ class glutathione transferasees, an invarient tyrosine is the catalytic base for deprotonating the incoming thiol-containing substrate and stabilizes the thiolate (*47*). Further biochemical studies will be aimed at exploring this hypothesis.

An interesting feature raised in the FPT mechanism is the fact that the zinc-bound cysteine thiolate from the bound CVIM peptide is ~7 Å from C1 of FPP in the FPT cocrystal structure (Figure 1). This distance must be reduced for alkylation to occur. In an associative electrophilic alkylation, conformational changes involving protein and/or ligands would be required to bring both the cysteine thiolate and C1 of FPP into proximity to initiate the reaction (Figure 6). One structural feature of the FPT ternary complex is that the distance from the thiolate to the endogenous zinc is 2.4 Å. This distance is longer than the average thiol−zinc bond (2.1 Å) measured in the Cambridge Small Molecule Database. If this longer thiol−zinc bond reflects a weaker interaction, then this may facilitate movement of the cysteine thiolate toward C1 of FPP. In addition, C1 of FPP may move toward the cysteine thiolate during the releasing of the diphosphate from FPP in the transition state.

Our steady-state kinetic analysis indicates that both single mutants, K164Nα and Y300Fβ, retain partial activity. In the proposed mechanism, each of the two residues helps stabilize the leaving group through protonation and/or hydrogen bonding. Removal of one will leave the other to assist the reaction. In addition, since the diphosphate moiety is an excellent leaving group, it is possible that the reaction proceeds spontaneously through propinquity catalysis (*48*) once the two substrates are close together.

On the basis of mutagenic studies, kinetic characterization, structural information, and previously reported biochemical studies, we propose that FPT proceeds through an associative electrophilic mechanism as shown in Figure 6. In this mechanism, K164α and Y300β are believed to play key catalytic roles in enhancing the reactivity of the leaving group. This mechanism is consistent with the current mechanistic studies of FPT. However, key questions of the reaction mechanism still remain to be confirmed, especially the function of Y300β as a general base and the conformational change required to overcome the 7 Å distance between C1 of FPP and the cysteine thiolate. Future biochemical studies such as the isotope effect studies with transient kinetic analysis and structural analysis of FPT with various substrates and products should further help to elucidate the FPT reaction mechanism.

ACKNOWLEDGMENT

We thank Dr. Patricia C. Weber for support of the project, Ms. Rosalinda Syto for assistance in protein purification, Dr. Yan-Hui Liu for performing the mass spectroscopic analysis, and Dr. Charles McNemar for N-terminal sequencing.

REFERENCES

1. Clarke, S. (1992) *Annu. Rev. Biochem. 61*, 355−386.
2. Gibbs, J. B., Oliff, A., and Kohl, N. E. (1994) *Cell 77*, 175−178.
3. James, G. L., Goldstein, J. L., Brown, M. S., Rawson, T. E., Somers, T. C., McDowell, R. S., Crowley, C. W., Lucas, B. K., Levinson, A. D., and Marsters, J. C. (1993) *Science 260*, 1937−1942.
4. Kohl, N. E., Mosser, S. D., Desolms, S. J., Giuliani, E. A., Pompliano, D. L., Graham, S. L., Smith, R. L., Scolnick, E. M., Oliff, A., and Gibbs, J. B. (1993) *Science 260*, 1934−1937.
5. Bishop, W. R., Bond, R., Petrin, J., Wang, L., Patton, R., Doll, R., Njoroge, G., Catino, J., Schwartz, J., Windsor, W., Syto, R., Schwartz, J., Carr, D., James, L., and Kirschmeier, P. (1995) *J. Biol. Chem. 270*, 30611−30618.
6. Kohl, N. E., Omer, C. A., Conner, M. W., Anthony, N. J., Davide, J. P., DeSolms, S. J., Giuliani, E. A., Gomez, R. P., Graham, S. L., Hamilton, K., Handt, K. L., Hartman, G. D., Koblan, K. S., Kral, A. M., Miller, P. J., Mosser, S. D., O'Neill, T. J., Rands, E., Schaber, M. D., Gibbs, J. B., and Oliff, A. (1995) *Nat. Med. 1*, 792−797.
7. Chen, W.-J., Andres, D. A., Goldstein, J. L., Russell, D. W., and Brown, M. S. (1991) *Cell 66*, 327−334.
8. Chen, W.-J., Andres, D. A., Goldstein, J. L., and Brown, M. S. (1991) *Proc. Natl. Acad. Sci. U.S.A. 88*, 11368−11372.
9. Omer, C. A., Kral, A. M., Diehl, R. E., Prendergast, G. C., Powers, S., Allen, C. M., Gibbs, J. B., and Kohl, N. E. (1993) *Biochemistry 32*, 5167−5176.
10. He, B., Chen, P., Chen, S.-Y., Vancura, K. L., Michaelis, S., and Powers, S. (1991) *Proc. Natl. Acad. Sci. U.S.A. 88*, 11373−11377.
11. Moores, S. L., Schaber, M. D., Mosser, S. D., Rands, E., O'Hara, M. B., Garsky, V. M., Marshall, M. S., Pompliano, D. L., and Gibbs, J. B. (1991) *J. Biol. Chem. 266*, 14603−14610.
12. Zhang, F. L., Diehl, R. E., Kohl, N. E., Gibbs, J. B., Giros, B., Casey, P. J., and Omer, C. A. (1994) *J. Biol. Chem. 269*, 3175−3180.
13. Yokoyama, K., McGeady, P., and Gelb, M. H. (1995) *Biochemistry 34*, 1344−1354.
14. Yokoyama, K., Goodwin, G. W., Ghomashchi, F., Glomset, J. A., and Gelb, M. H. (1991) *Proc. Natl. Acad. Sci. U.S.A. 88*, 5302−5306.
15. Zhang, F. L., and Casey, P. J. (1996) *Annu. Rev. Biochem. 65*, 241−269.
16. Pompliano, D., Schaber, M., Mosser, S., Omer, C., Shafer, J., and Gibbs, J. (1993) *Biochemistry 32*, 8341−8347.
17. Furfine, E., Leban, J., Landavazo, A., Moomaw, J., and Casey, P. (1995) *Biochemistry 34*, 6857−6862.
18. Mathis, J., and Poulter, C. (1997) *Biochemistry 36*, 6367−6376.
19. Cassidy, P. B., and Poulter, C. D. (1996) *J. Am. Chem. Soc. 118*, 8761−8762.
20. Dolence, J., and Poulter, C. (1995) *Proc. Natl. Acad. Sci. U.S.A. 92*, 5008−5011.
21. Huang, C.-C., Casey, P. J., and Fierke, C. A. (1997) *J. Biol. Chem. 272*, 20−23.
22. Hightower, K. E., Huang, C.-C., Casey, P. J., and Fierke, C. A. (1998) *Biochemistry 37*, 15555−15562.
23. Mu, Y., Omer, C., and Gibbs, R. (1996) *J. Am. Chem. Soc. 118*, 1817−1823.

24. Strickland, C. L., Windsor, W. T., Syto, R., Wang, L., Bond, R., Wu, Z., Schwartz, J., Le, H. V., Beese, L. S., and Weber, P. C. (1998) *Biochemistry 37*, 16601−16611.
25. Long, S. B., Casey, P. J., and Beese, L. S. (1998) *Biochemistry 37*, 9612−9618.
26. Wu, Z., Demma, M., Strickland, C., Syto, R., Le, H., Windsor, W. T., and Weber, P. C. (1999) *Protein Eng. 12*, 341−348.
27. Ho, S. N., Hunt, H. D., Horton, R. M., Pullen, J. K., and Pease, L. R. (1989) *Gene 77*, 51−59.
28. Bradford, M. M. (1976) *Anal. Biochem. 72*, 248−254.
29. Johnson, K. A. (1986) *Methods Enzymol. 134*, 677−705.
30. Kral, A. M., Diehl, R. E., deSolms, S. J., Williams, T. M., Kohl, N. E., and Omer, C. A. (1997) *J. Biol. Chem. 272*, 27319−27323.
31. Villar, K. D., Mitsuzawa, H., Yang, W., Sattler, I., and Tamanoi, F. (1997) *J. Biol. Chem. 272*, 680−687.
32. Andres, D. A., Goldstein, J. L., Ho, Y. K., and Brown, M. S. (1993) *J. Biol. Chem. 268*, 1383−1390.
33. Dougherty, D. A. (1996) *Science 271*, 163−168.
34. Dolence, J. M., Cassidy, P. B., Mathis, J. R., and Poulter, C. D. (1995) *Biochemistry 34*, 16687−16694.
35. Karshikoff, A., Reinemer, P., Huber, R., and Ladenstein, R. (1993) *Eur. J. Biochem. 215*, 663−670.
36. Schlegel, B. P., Ratnam, K., and Penning, T. M. (1998) *Biochemistry 37*, 11003−11011.
37. Matthews, R. G., and Goulding, C. W. (1997) *Curr. Opin. Chem. Biol. 1*, 332−339.
38. Gonzalez, J. C., Peariso, K., Penner-Hahn, J. E., and Matthews, R. G. (1996) *Biochemistry 35*, 12228−12234.
39. Myers, L. C., Verdine, G. L., and Wagner, G. (1993) *Biochemistry 32*, 14089−14094.
40. Poulter, C. D., and Rilling, H. C. (1978) *Acc. Chem. Res. 11*, 307−313.
41. Cane, D. E. (1990) *Chem. Rev. 90*, 1089−1103.
42. Wendt, K. U., and Schulz, G. E. (1998) *Structure 6*, 127−133.
43. Jencks, W. P. (1981) *Chem. Soc. Rev. 10*, 345−375.
44. Weller, V. A., and Distefano, M. D. (1998) *J. Am. Chem. Soc. 120*, 7975−7976.
45. Ellsworth, B. A., Tom, N. J., and Bartlett, P. A. (1996) *Chem. Biol. 3*, 37−44.
46. Tarshis, L., Proteau, P., Kellogg, B., Sacchettini, J., and Poulter, C. (1996) *Proc. Natl. Acad. Sci. U.S.A. 93*, 15018−15023.
47. Caccuri, A. M., Antonini, G., Nicotra, M., Battistoni, A., Bello, M. L., Board, P. G., Parker, M. W., and Ricci, G. (1997) *J. Biol. Chem. 272*, 29681−29686.
48. Jencks, W. P. (1975) in *Advances in Enzymology and Related Areas of Molecular Biology* (Meister, A., Ed.) p 43, John Wiley & Sons, Inc., New York.

BI990583T